

# Estimating the Temperature Experienced by Biomass Particles during Fast Pyrolysis Using Microscopic Analysis of Biochars

Logan C. Thompson, Peter N. Ciesielski, Mark W. Jarvis, Calvin Mukarakate, Mark R. Nimlos, Mark R. Nimlos, and Bryon S. Donohoe\*,\*

<sup>†</sup>National Bioenergy Center, <sup>‡</sup>Biosciences Center, National Renewable Energy Laboratory, Golden, Colorado 80401, United States

Supporting Information

ABSTRACT: Biomass particles can experience variable thermal conditions during fast pyrolysis due to differences in their size and morphology, and from local temperature variations within a reactor. These differences lead to increased heterogeneity of the chemical products obtained in the pyrolysis vapors and bio-oil. Here we present a simple, high-throughput method to investigate the thermal history experienced by large ensembles of particles during fast pyrolysis by imaging and quantitative image analysis. We present a correlation between the surface luminance (darkness) of the biochar particle and the highest temperature that it experienced during pyrolysis. Next, we apply this correlation to large, heterogeneous ensembles of char particles produced in a laminar entrained flow reactor (LEFR). The results are used to interpret the actual temperature distributions delivered by the reactor over a range of operating conditions.

### ■ INTRODUCTION

The increasing global demand for energy and the necessity to reduce global greenhouse emissions has made overcoming technical challenges in the conversion of lignocellulosic biomass into drop-in biofuels a top socioeconomic concern.<sup>1,2</sup> Among the biomass conversion technologies, fast pyrolysis has emerged as a promising route for commercial conversion of biomass from energy crops, agricultural waste and forestry residues into liquid hydrocarbons for fuels and chemicals.<sup>3,4</sup> Fast pyrolysis involves rapidly heating (~1000 °C/sec) biomass in an anoxic environment to depolymerize and vaporize the biopolymers that compose biomass particles. Condensation of the pyrolysis vapors produces a liquid mixture of hydrocarbons, carbohydrates, and water, collectively referred to as bio-oil. 5,6 Several studies have shown that the overall carbon yield and bio-oil composition are affected by several feedstock characteristics such as particle size<sup>7</sup> and plant species,<sup>8,9</sup> and especially by process factors such as heating rate and residence time.<sup>10,11</sup> Decoupling these variables in experiments that replicate realistic biomass fast pyrolysis conditions to probe their impact on the outcomes is challenging. 12

Variation in the actual heating rate and final temperature experienced by individual biomass particles due to reactor and process variables can activate chemical reactions that proceed through different mechanisms. 13 This manifests as decreased yields and increased heterogeneity of chemical species present in the bio-oil. Under ideal conditions the heating profile and residence time of every biomass particle in a pyrolysis reactor would be identical during the entire fast pyrolysis process. In practice, however, some variation in heating conditions experienced by individual particles is inevitable. 14-17 Understanding the impact, and being able to predict this heterogeneity would facilitate optimization of fast pyrolysis process conditions. Therefore, establishing methods to quickly and easily estimate the temperature conditions experienced by individual biomass particles and ensembles of particles during fast pyrolysis is important to attain consistent, repeatable biomass conversion process conditions.

Here we present a relatively simple, imaging-based approach to probe the consistency of pyrolysis process conditions by a surface evaluation of the residual char particles. Previous studies of biomass and char particles in the context of fast pyrolysis have often focused on an in-depth characterization of only a few particles. 18,19 Others have used optical measurements to correlate reactor temperature and particle morphology in biomass and coal combustion experiments. 20,21 A higher throughput, repeatable method for investigating the thermal history of a statistically significant number of particles is desirable. In this study, we derive a correlation that relates the visible light surface reflected luminance of postpyrolysis biochar particles to the temperature at which the particles were pyrolyzed in a small, well controlled, thermostable, horizontal flow reactor. The correlation is then applied to large sample sets of biochar particles produced in a laminar entrained flow reactor (LEFR), allowing for the highest temperature experienced during fast pyrolysis to be estimated simultaneously for a large sample of biomass particles.

## RESULTS AND DISCUSSION

Heterogeneity Color and Morphology in Char Particles Obtained from Laboratory Scale Pyrolysis Reactors. Figure 1 shows a magnification series obtained by reflected light stereomicroscopy of two different char samples obtained from continuous feed LEFR experiments. The milled pine biomass particles, sieved to size ranges of 40-60 mesh  $(425-250 \mu m)$  and 40-45 mesh  $(425-355 \mu m)$  were each pyrolyzed with the reactor temperature set to 500 °C and an expected residence time of 6-7 s. This is a common pyrolysis

Received: March 20, 2017 Revised: June 7, 2017





Figure 1. Reflected light stereoscope micrographs of unsorted pine chars. Two different size ranges, 40-60 mesh and 40-45 mesh, of milled loblolly pine particles were subjected to fast pyrolysis at 500 °C. The char particles display color and morphological heterogeneity suggesting they were subjected to pyrolysis under variable process conditions.

temperature and residence time that achieves high yields of biooil and a particle size range that should not be in the thermally thick regime.<sup>22</sup> Both char samples display heterogeneity in color and morphology. Some particles appear very similar to unpyrolyzed biomass in color and shape. Other particles are entirely black and appear smaller, frayed, and twisted compared to native biomass particles. Some char particles display evidence of having transitioned through a melt phase and share little morphology with the original biomass particles. 23,24 These morphological changes are most obvious in the images obtained at the highest magnification presented in the bottom row of Figure 1. Resolving information about this heterogeneous char mixture will allow for a more detailed understanding of what conditions individual biomass particles experience inside this LEFR pyrolysis reactor and is the motivation for the analysis and methods presented here.

Relationships between Char Color and Morphology and the Temperature They Experienced Elucidated by Controlled Temperature Pyrolysis Experiments. To better understand the heterogeneous biochars exiting continuous-feed reactors such as those shown in Figure 1, the same biomass feedstock was pyrolyzed in a tightly temperature controlled, batch-fed reactor at smaller scale in order to determine what combinations of time and temperature are responsible for the range of char colors and morphology observed in the LEFR chars. The results of this analysis are shown in Figure 2. As both residence time and reactor temperature increase, the chars show a gradient of color and morphological change. The pine pyrolyzed at the highest

temperature and lowest residence time (550 °C, 11 s) appears very similar to the pine pyrolyzed at the lowest temperature but highest residence time (400 °C, 90 s) and only when both residence time and reactor temperature are sufficiently high does the complete set of biochar particles display color and morphology consistent with having undergone effective pyrolysis. In the bottom right corner of Figure 2, where both temperature and residence time are high, chars are completely darkened and show the same frayed and twisted morphology seen in some of the particle shown in Figure 1. These results provide qualitative comparisons between known pyrolysis conditions and resulting chars to help better understand what conditions individual char particles may have experienced inside a continuous feed reactor where local reactor conditions may have varied.

Figure 3 shows a representative vapor pulse from the molecular beam mass spectrometer (MBMS) revealing that at 500 °C the length of time for the complete pyrolysis of a 25 mg sample of milled pine in a quartz boat was 90 s. The timing of a pulse began once the biomass was first inserted into the heated reactor; however, it takes several seconds for volatilization to begin because heat transfer limitations prevent particles from instantaneously reaching volatilization temperatures, and the timing extended along the tail of the vapor pulse peak until spectral analysis showed all volatilization had ended. This heating time duration also fits with recent work showing that all the biomass particles require longer heating times for complete devolitilization than is usually presumed.<sup>2</sup>

Additional Physical Evidence of Morphological Change Revealed by Scanning Electron Microscopy Imaging (SEM) of Temperature-Controlled Standards. In addition to the temperature standards pyrolyzed in the batchfed reactor shown in Figure 2, other standards were pyrolyzed in the range 200–600 °C until the samples at each temperature achieved steady state and cessation of vapor production from the sample was observed by real-time MBMS. Figure 4 displays SEM micrographs of those chars. The microscale morphology of chars that experienced temperatures below that of typical pyrolysis (200-400 °C) was largely similar to that of native biomass particles. In these samples, the long, tubular structures characteristic of pine fiber cells and perforated walls of vessel elements can be identified. Their morphology remained relatively unchanged in samples that experienced temperatures ≤ 400 °C. However, cellular deformation, particle fraying, and fracture are evident in samples pyrolyzed at temperatures of 500 °C and higher. Instances where cellular features are bent or otherwise deformed likely arise from changes in the viscoelastic properties of the biomass particles as they pass through a melt phase during pyrolysis. While changes in structural features that result from temperatures ≥ 500 °C may be observed by SEM, little or no differences are observed to result from temperatures between 200 and 400 °C. This observation suggests the luminance analysis by light microscopy is a more effective tool for identifying the temperature experienced by biomass particles over this temperature interval.

**Empirical Correlation between Known Temperature** Values and Observed Darkness Values. To further analyze the 200-600 °C temperature standards the chars were imaged by reflected light stereoscope imaging. An empirical correlation was obtained to quantitatively relate the grayscale intensity values displayed by the char particles in the stereomicrographs and the temperature at which they were pyrolyzed. In general, the grayscale values obtained for char particles changed linearly

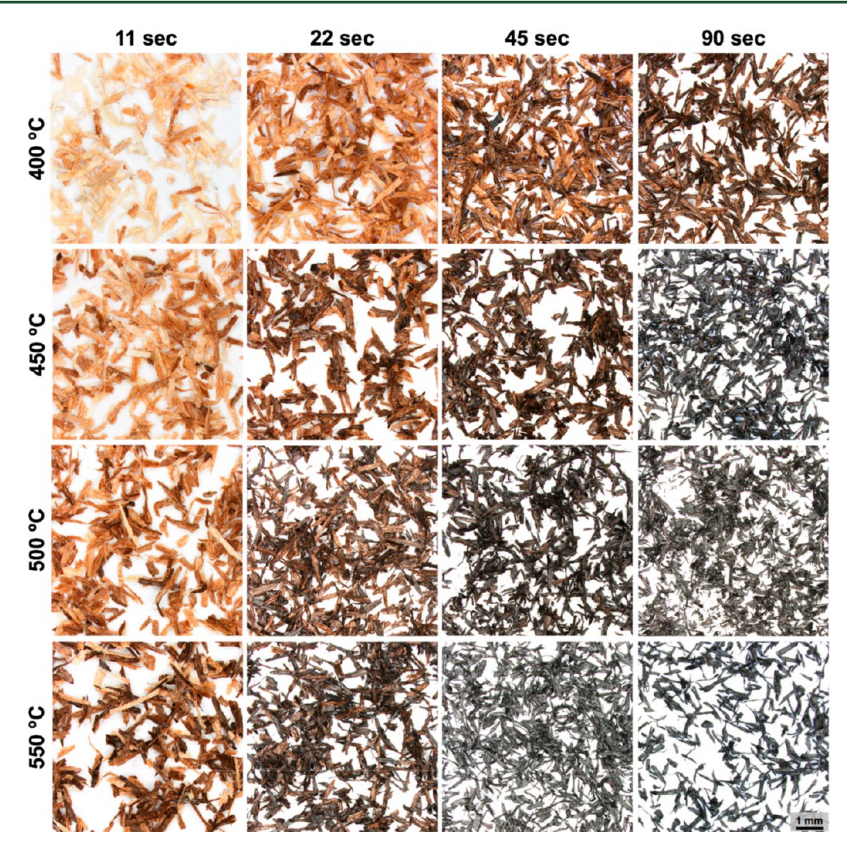


Figure 2. Reflected light stereoscope micrographs of loblolly pine wood particles after fast pyrolysis in a horizontal reactor at tightly controlled temperatures from 400 °C-550 °C and in a time series from 11 to 90 s residence times from the onset of volitilization. Char particles within each treatment display a rather homogeneous surface color and morphology. Across the range of conditions, samples show gradients of color change from light brown to black as well as developing morphological changes such as shrinking and fragmentation.

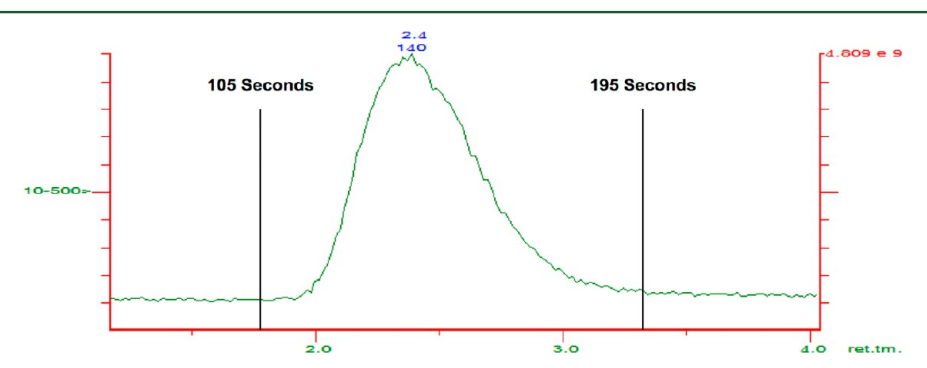


Figure 3. Total ion count (TIC) trace of a single molecular beam mass spectrometer (MBMS) vapor pulse from 25 mg of 40-60 mesh milled pine biomass pyrolyzed at 500 °C. This demonstrates that 90 s is sufficient for complete pyrolysis in the horizontal reactor used to generate the controlled temperature standards.

over the temperature range of 200–400  $^{\circ}\text{C}$ , and approached an asymptote beginning around 500 °C. To capture this behavior, we employed an expression for the grayscale value of the chars that was an exponential function of the temperature at which they were pyrolyzed:

$$G = G_{\text{max}} \{ 1 - \exp[k(G_{\text{min}} - T)] \}$$
 (1)

where G is the grayscale value,  $G_{\text{max}}$  is the maximum possible grayscale value (i.e., 256 for 8-bit grayscale images), k is an empirically obtained proportionality constant,  $G_{\min}$  is the minimum grayscale value predicted by the function, and T is the temperature in °C. Equation 1 may be rearranged to yield an expression for T as a logarithmic function of the grayscale value as

$$T = -k \log \left( \frac{G_{\text{max}} - G}{G_{\text{max}}} \right) + G_{\text{min}}$$
 (2)

Values for k and  $G_{min}$  were obtained by a least-squares regression of eq 2 using the grayscale values obtained from the micrographs of char particles that were pyrolyzed at each T value. However, because of the asymptotic behavior of the grayscale values observed at temperatures above 500 °C, we chose to only consider T values (and corresponding G values) on the interval [200, 500] in the regression analysis in order to achieve the maximum sensitivity in this range since differentiating temperatures in this regime is paramount to evaluating the effectiveness of fast pyrolysis process conditions. However, this approach does come at the expense of sensitivity

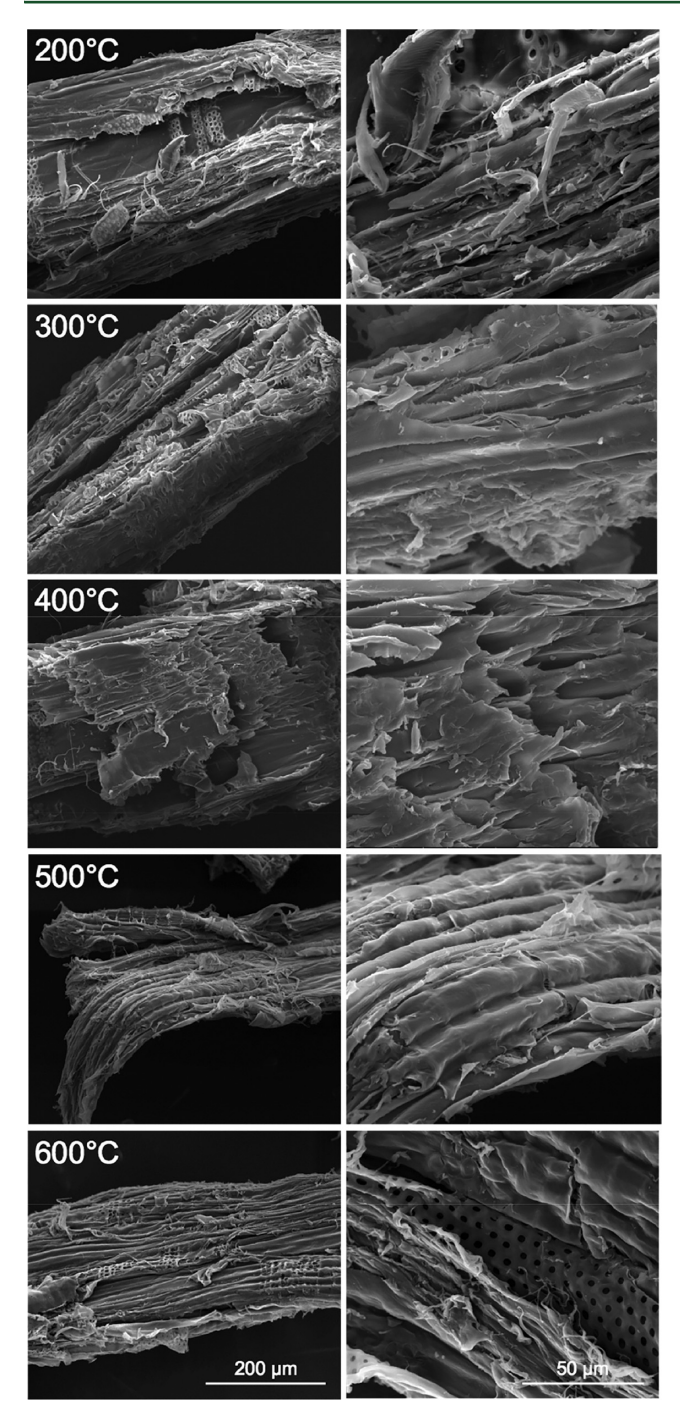


Figure 4. Scanning electron micrographs (SEM) of milled loblolly pine char particles pyrolyzed in the horizontal reactor at controlled temperatures between 200 and 600 °C for 90 s. All of the chars retain the general microstructure of pine wood with distinct cell lumen and cell walls remaining. There is evidence for particle shrinkage and smoothing of the char cell walls observed in the 500 and 600 °C pyrolyzed samples.

at temperatures above 500 °C since these data points were intentionally omitted from the regression analysis to enhance sensitivity at lower temperatures. Therefore, the empirical relationship described by eq 2 provides reasonable estimates for the temperature experienced by particles on the interval [200, 500], but the relationship may not be extrapolated to differentiate temperatures > 500  $^{\circ}$ C. In other words, all temperatures predicted to fall in this range should simply be

classified as > 500 °C. This empirical fit is plotted with the experimental data from which it was derived in Figure 5. Insets

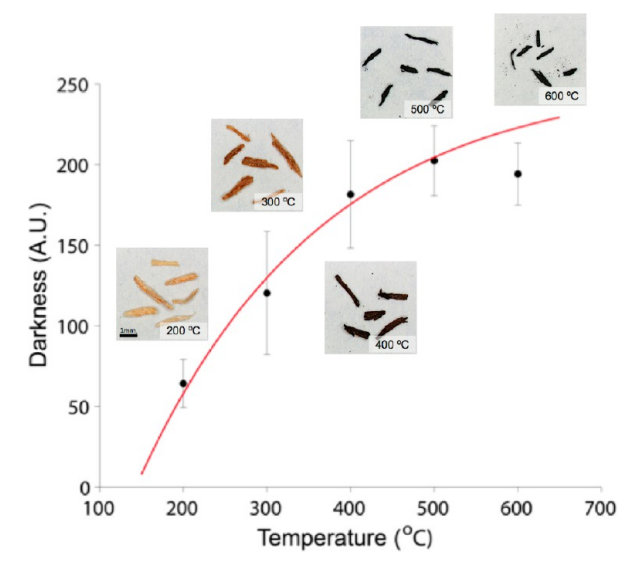
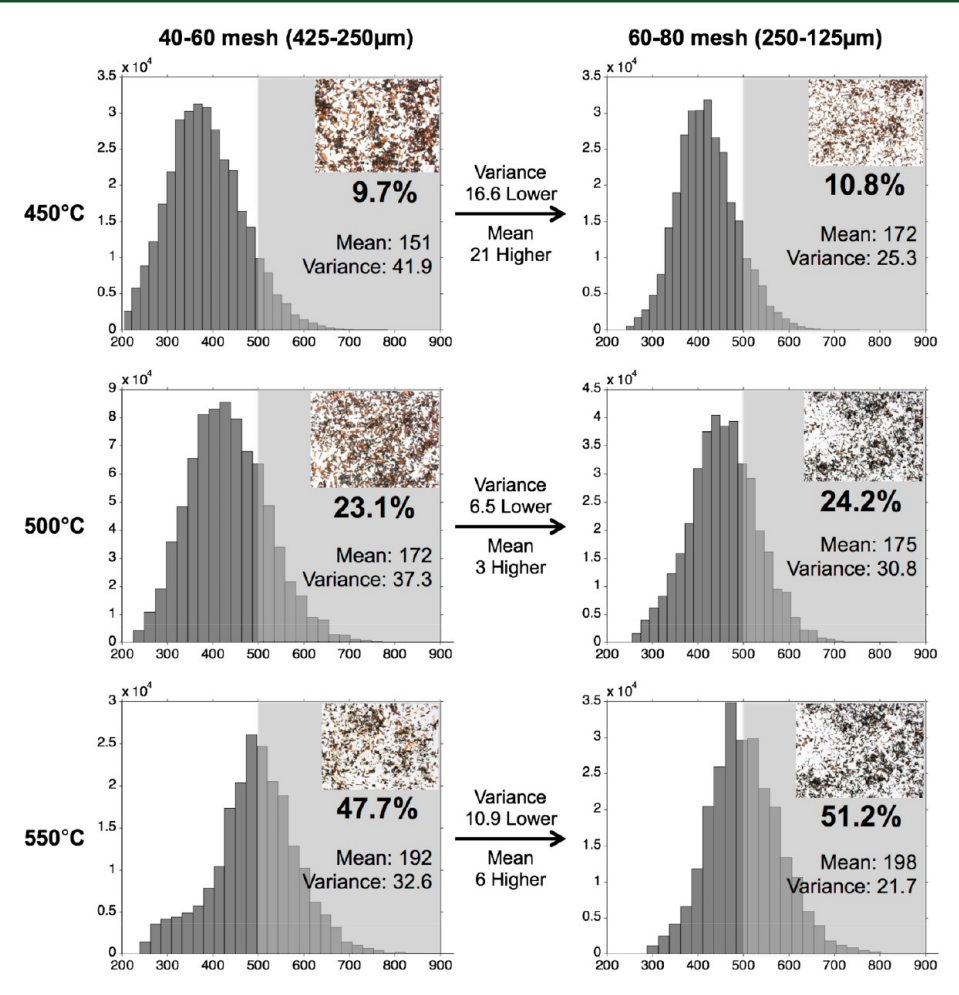


Figure 5. Luminance (reported as darkness = 256-luminance) values of biomass chars were used to generate a fitted curve that can be used to estimate the actual temperature experienced by chars from any pyrolysis reactor based on the loss of surface luminance of the chars as they experience increasing reactor temperatures. The darkness values are derived from reflected light stereoscope micrographs of char particles after pyrolysis in a horizontal reactor at temperatures from 200 °C−600 °C.

show examples of color images from which grayscale values were obtained at each temperature. The best-fit parameters for k and  $G_{\min}$  obtained from least-squares regression of these data are 200.9768 and 186.2754, respectively.

To validate that the curve fitting used to analyze LEFR chars yielded reliable and repeatable numbers, multiple samplings were taken from each char sample to compare estimation of mean darkness value and variance, shown in Figure S2. Four rounds of sampling with replacement from the 60-80 mesh  $(250-125 \mu m)$  particles pyrolyzed in the LEFR reactor set at 550 °C demonstrate an estimated mean darkness of 198.3 °C  $\pm$ 2.7 and an estimated variance of 21.7 °C  $\pm$  0.2, meaning that both values vary by less than 1.5% of the value of the estimate. The samples also yielded similar estimations for the fraction of biomass that reached an effective pyrolysis threshold of 500 °C with an average of  $51.2\% \pm 3.8\%$ . Estimations of mean darkness value, variance, and fraction of biomass above 500 °C were similarly consistent for all other temperature controlled standards.

Darkness Correlation Estimation of the Distribution of Temperatures Experienced by Chars Pyrolyzed in the Continuous-Feed LEFR. Milled pine of sizes 40-60 mesh  $(425-250 \mu m)$  and 60-80 mesh  $(250-125 \mu m)$  pyrolyzed in the LEFR reactor with midpoint gas temperatures of 450 °C, 500 °C, and 550 °C were analyzed to determine how consistently the population of particles actually experienced the intended pyrolysis temperature (Figure 6). As described above, estimating temperatures above 500 °C is not accurate with this model; however, because the particles temperature can be estimated at ≤500 °C it is possible to say what temperature particles at <500 °C reached as well as what percentage of the sample reached any threshold temperature at



**Figure 6.** Histograms of darkness value distributions and corresponding statistics for char particles pyrolyzed at 450 °C, 500 °C, and 550 °C. Gray boxes show the percentage of biomass that reached an effective pyrolysis threshold of 500 °C. The mean darkness value is higher and the variance around the mean is lower for the 60–80 mesh particles than the 40–60 mesh particles at all three pyrolysis temperatures.

or below 500  $^{\circ}\text{C}$ . Here 500  $^{\circ}\text{C}$  was chosen as the threshold temperature because it is a common and effective pyrolysis temperature and MBMS vapor analysis shows that above 500 °C the mean ion count does not continue to increase, indicating that volatilization has completed. An ideal pyrolysis run would see 100% of biomass particles reach the threshold temperature. When the continuous-fed LEFR reactor was set to 500 °C and measuring 500 °C as the constant midgas stream temperature, less than 25% of particles actually reached that temperature. This might mean the residence time was too low, the particle size too large, or a higher temperature was necessary to transfer enough heat to biomass particles of this size within the residence time to achieve the desired pyrolysis conditions for all particles. More broadly, this demonstrates that even when a continuous-fed reactor is well tuned and delivering a gas stream at the desired temperature, that does not necessarily mean that biomass particles are reaching that temperature. Insufficient residence time in a properly heated reactor, irregularities in the laminar profile creating local areas where the gas is not maintaining temperature, or both would lead to the population of biomass not pyrolyzing at the temperature a reactor is producing.

Between the two particle size ranges tested, the temperature distribution estimated for 60–80 mesh particles is significantly narrower than that of the larger 40–60 mesh particles, with a variance on average 11.3 lower. The 60–80 mesh particles also

displayed a mean darkness on average 10.0 higher. All three of the 60–80 mesh chars contained a larger percentage of biomass particle above the 500 °C threshold than the 40–60 mesh chars at the same temperature. The smaller particles likely provide lower heat and mass transfer limitations and facilitate more complete pyrolysis during the short residence times of fast pyrolysis. A smaller particle size having higher mean darkness, lower distribution variance, and higher percentage of biomass above 500 °C suggests that for the LEFR and likely for any pyrolysis reactor, at any given residence time there is a maximum allowed particle size in order to achieve effective fast pyrolysis.

As the temperature increases the variance tends to decrease, with the exception of comparing the 450 to 500 °C temperature for the 60–80 mesh particles; however, from 450 to 550 °C the trend is clear that the variance is decreasing with increasing temperature. Figure 7 provides a possible explanation for why the variance might decrease as temperature increases. At temperatures below those typical for effective biomass pyrolysis, such as 400 °C, the char darkens inconsistently with some particles darkening faster than others and even inconsistent darkening across an entire particle. However, at higher temperatures such as 550 °C particles that appear fully pyrolyzed are homogeneously darkened across the entire particle. Higher temperatures create a higher proportion of particles that are completely dark which leads to lower

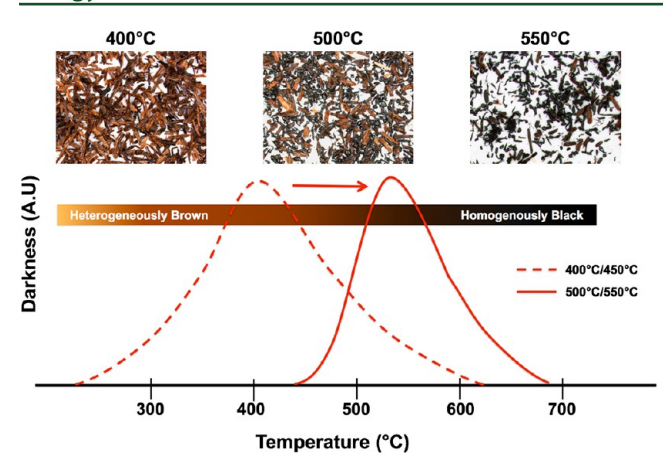


Figure 7. Illustration of how an increase in reactor temperature from a 400 °C-450 °C range to a 500 °C-550 °C range correlates with a decrease in variance around the mean darkness value of the biomass particles exposed to the higher temperatures.

variance in the population of particles. It should also be noted however that because the empirical fit model approaches an asymptote around 500 °C, the model would also predict lower variance at higher temperatures.

Particle-Scale Pyrolysis Model and Additional Insight into the Heating and Conversion Behavior Exhibited by Particles in the Entrained Flow Reactor System. The particle model geometry (shown in Figure 8A) was modeled in

three dimensions using realistic dimensions obtained from image analysis as described previously. 26,27 A Feret diameter of 1 mm was chosen to represent a particle of typical dimensions used in this study (we note that biomass particles often have Feret diameters substantially larger than the sieve mesh size due to their high aspect ratio). The model consisted of a classic pyrolysis reaction scheme coupled to an implementation of the Navier-Stokes wherein Darcy's Law was used to approximate fluid flow within the porous particle. The reaction scheme employed was that developed by Di Blasi<sup>28</sup> and colleagues which tracks the conversion of pine wood into char and lumped product classes of light gases and condensable vapors (often referred to as tar or bio-oil) while accounting for secondary reactions by which condensable vapors may crack to light gases and recondense to form additional char. The reaction kinetics are given in the form of Arrhenius expressions. The conservation equations for energy, mass, and momentum are respectively given by

$$\rho C_p \frac{\partial T}{\partial t} = \nabla \cdot (k \nabla T) - \rho C_p \mathbf{u} \cdot \nabla T + Q$$
(3)

$$\varepsilon_{\mathbf{p}} \frac{\partial c_i}{\partial t} + \nabla \cdot (-D_i \nabla c_i) + \mathbf{u} \cdot \nabla c_i = R_i$$
(4)

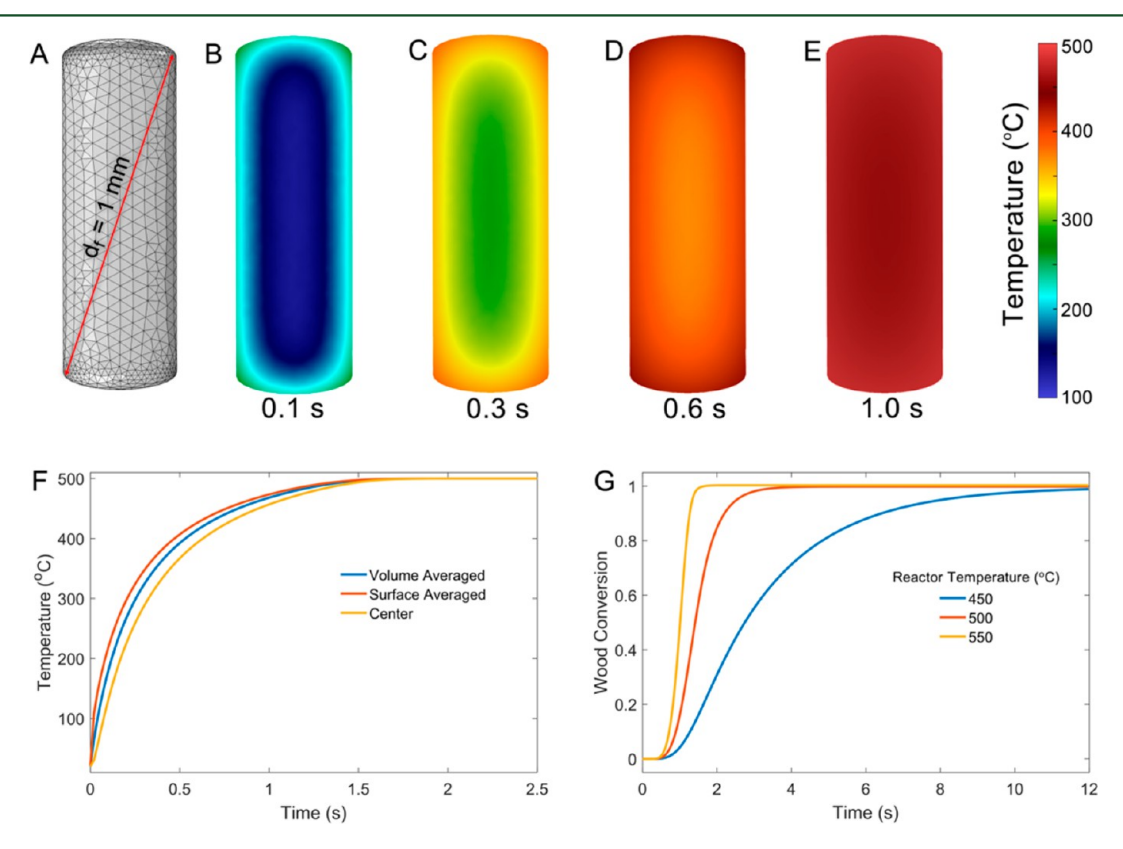


Figure 8. Particle-scale modeling results. (A) Meshed particle geometry used in the simulations; df denotes Feret diameter. (B-E) Longitudinal slices through the center of the particle obtained from the simulation with a reactor temperature 500 °C show small thermal gradients that persist within the particle throughout the first second of simulation time. (F) Plots of the volume averaged, surface averaged, and center temperature of the particle obtained from the simulation with a reactor temperature 500 °C show that the particle temperature becomes isothermal shortly after 1.5 s of simulation time. (G) Plots of the wood conversion vs time obtained from simulations with reactor temperatures of 450 °C, 500 °C, and 550 °C highlight the disparity in reaction kinetics observed in these different temperature regimes.

$$\frac{\rho}{\varepsilon_{p}} \left( \frac{\partial \mathbf{u}}{\partial t} + (\mathbf{u} \cdot \nabla) \frac{\mathbf{u}}{\varepsilon_{p}} \right)$$

$$= -\nabla p + \nabla \cdot \left\{ \frac{1}{\varepsilon_{p}} \left( \mu (\nabla \mathbf{u} + (\nabla \mathbf{u})^{T}) - \frac{2}{3} \mu (\nabla \cdot \mathbf{u}) \mathbf{I} \right) \right\}$$

$$- \left( \kappa_{ij}^{-1} \mu + \frac{\rho \nabla \cdot \mathbf{u}}{\varepsilon_{p}^{2}} \right) \mathbf{u}$$
(5)

where  $\rho$  is the density,  $C_P$  is the heat capacity at constant pressure, T is the temperature, k is the thermal conductivity,  $\mathbf{u}$ the velocity vector, Q is the heat generation term,  $c_i$  is the concentration species i,  $D_i$  is the diffusion coefficient for species *i*,  $R_i$  is the sum reaction rates for species *i*,  $\varepsilon_p$  is the porosity,  $\mu$  is the viscosity, I is the identity matrix,  $\kappa_{ij}$  is the permeability tensor, and the superscript T in eq 5 denotes the transpose operator. The heat capacity, thermal conductivity, density, and viscosity were calculated at each time step as the mass-fractionweighted sum of properties of the components present within each element. The boundary conditions for eq 4 were given by  $-\mathbf{n}\cdot D_i \nabla c_i = 0$  (where **n** is the unit normal vector) for all species at the particle boundary. The boundary condition for eq 5 was given by p = 1 atm at the particle boundary. The boundary condition for eq 3 was given by

$$q_{\text{interface}} = h(T_{\text{s}} - T_{\infty}) \tag{6}$$

where h is interfacial heat transfer coefficient,  $T_S$  is the surface temperature of the particle, and  $T_{\infty}$  approximates the operating temperature of the reactor in this scenario. The heat transfer coefficient was obtained by estimating the local flow regime experienced by the particle, and thereby the particle Reynolds number and Prandtl number of the surrounding vapor, as we described recently.<sup>29</sup> The terminal velocity of the particle falling through the reactor was estimated to be ~0.5 m/s using a force balance as described by Ellens.<sup>30</sup> The Sauter diameter, defined as  $D_S = V^3/A^2$  (where V and A are the volume and surface area of the particle, respectively) was taken as the equivalent spherical diameter for the terminal velocity estimation. The Reynolds number was calculated to be 59, which indicates that velocity field in the vicinity of the particle is indeed in the laminar regime. The Prandtl number of nitrogen at 1 atm and 500 °C was calculated to be 0.72. These two dimensionless numbers provided an estimate for the heat transfer coefficient of 550 W/(m<sup>2</sup>·°C) by interpolation of previously computed values.<sup>29</sup> Simulations were performed using  $T_{\infty}$  values of 450 °C, 500 °C, and 550 °C.

Temperature profiles visualized at the longitudinal cross section through the center of the particle obtained at various points throughout the initial heating phase of the simulation performed with  $T_{\infty}$  = 500 °C are presented in Figure 8B–E. These slices show that relatively small thermal gradients are present within the particle during the initial heating stages, with the narrow edges at the particle extremities heating more quickly than the interior as expected. Plots of the volumeaveraged, surface-averaged, and center temperature profiles from the same simulation are shown in Figure 8F. These plots indicate that the volume-averaged and surface-averaged temperatures remain within ~20 °C throughout the particle heating time. These observations are consistent with the Biot number of 0.24 (computed as  $Bi = V/A \cdot h/k$ ) obtained for the particle model employed in these simulations, which is slightly larger than the heuristic value of 0.1 at which the internal spatial thermal gradients may be neglected. Finally, these plots indicate that the particle becomes isothermal after ~1.5 s at which pyrolysis reactions begin to occur homogeneously throughout the particle.

The conversion of wood into pyrolysis products obtained at each simulation temperature is presented in Figure 8G. These results predict complete conversion of the particle in <2 s at a reactor temperature of 550 °C, 4 s at 500 °C, and 12 s at 450 °C. However, the time at the onset of the simulation wherein no conversion is observed as the particle reaches pyrolysis temperatures is largely similar for each of the different temperatures. This observation indicates that the large disparities in the conversion times predicted for these operating temperatures are largely a function of the kinetic rates, which depend exponentially on temperature, rather than the heat transfer limitations. Combining these predictions with the expected residence time distribution delivered by the reactor provides additional insight into the origin of the heterogeneity in the extent of pyrolysis displayed by the particles at certain conditions. The LEFR used for these experiments has an inner diameter of 1.37 in. and was operated with a carrier gas flow rate of 6.5 SLPM, which equates to an approximate nominal gas velocity of 0.11 m/s. Dividing the length of the reactor (30 in.) by this nominal gas velocity provides an estimate of the average gas residence time of 6.7 s. However, only very small particles experience this residence time, while larger particles are accelerated by gravity, reducing their residence time. This is qualitatively evident in the images of larger biochar particles pyrolyzed in the LEFR that appear lighter than smaller particles, indicating their relatively shorter residence times. In addition, the pyrolysis vapors emitted by the particle introduce additional vapor volume, which will act to accelerate the gas velocity through the reactor and further reduce the residence time of the particles. A detailed CFD model of residence time distributions in the LEFR that accounts for the aforementioned complexities is beyond the scope of the present work; however, some general observations may be made by considering the conversion predictions presented in Figure 8G and the analysis of the larger particles presented on the left side of Figure 6. The small population (9.7%) of particles that were effectively pyrolyzed in 450 °C LEFR experiment were likely the smallest particles that became entrained near the edges of the reactor where the carrier gas velocity was the slowest and heat transfer was highest. The larger population (23.1%) of particles that were effectively pyrolyzed in 500 °C experiment were also likely small particles that experienced longer residence times in the reactor of at least 3.5-4 s. The 550 °C experiment produced the largest population of effectively pyrolyzed particles, which is expected based on the relatively short (<3 s) conversion time predicted by the simulation; however, a significant population of particles (52.3%) did not effectively pyrolyze which indicates that these particles experienced residence times of <2 s in the reactor. These are likely large particles with relatively fast slip velocities that were present near the center of the reactor where the fluid velocity is the highest and heat transfer is low relative to locations in close proximity to the reactor wall.

#### CONCLUSIONS

A simple optical imaging technique and digital image analysis were used to quickly estimate the percentage of biomass that attained a desired pyrolysis threshold of 500 °C during fast pyrolysis. Char particles generated during pyrolysis in a

controlled-temperature, batch-fed reactor demonstrated a clear gradient of color and morphological changes on both temperature and residence time gradients that underlie the heterogeneity observed in chars from a continuous-fed reactor. Similar char samples produced in the controlled-temperature, batch-fed reactor were then used to generate an empirical relationship that could estimate the temperature of char samples from any reactor. The resulting empirical fit model was used to estimate the temperature attained by particles below 500 °C and to estimate the percentage of biomass that attained a desired temperature threshold of 500 °C inside a continuous-feed LEFR fast pyrolysis reactor. A particle scale pyrolysis model was developed to provide additional insight into the pyrolysis scenarios delivered by the LEFR at various temperatures. The model provided quantitative estimates of the conversion extent of a representative particle as a function of residence time and reactor temperature, as well as some qualitative observations about the expected behavior of particles within the reactor.

## ■ MATERIALS AND METHODS

Biomass Sample Preparation. Biomass particles were prepared by knife milling (Wiley Knife Mill) five year old, debarked, loblolly pine tree slabs. The milled biomass was sieved to four particles size ranges; 35-40 mesh (500-425  $\mu$ m), 40-45 mesh (425-355  $\mu$ m), 40-60 mesh ( $425-250 \mu m$ ), and 60-80 mesh ( $250-125 \mu m$ ).

Horizontal Reactor Experiments. This reactor system was used to generate pyrolysis chars over a range of temperatures to serve as a training set from which empirical relationships between char characteristics and pyrolysis temperature could be obtained. The reactor system consisted of a horizontal quartz annular flow tube reactor coupled with a molecular beam mass spectrometer (MBMS).<sup>3</sup> Batch-wise pyrolysis and vapor upgrading took place in the inner tube where the vapors were carried in a 0.4 SLM flow of helium. The flow in the inner tube was mixed with a 4 SLM helium flow from the outer tube at the end of the reactor and before being sampled by the MBMS orifice. Diluting with the outer flow reduces secondary reactions and meets the flow demands of the sampling orifice. Quartz boats containing 25 mg samples of biomass were introduced into the heated flow in the inner tube. The reactor was heated to the desired temperature using a five-zone furnace. The vapors from each pulse were then sampled at the MBMS orifice.

The sampled gases undergo adiabatic expansion through a 250  $\mu m$ orifice into a vacuum chamber held at ~100 mTorr. This expansion cools the gas and effectively prevents subsequent chemical reactions. The cooled gas is skimmed into a molecular beam and is then ionized with an electron impact ionization source of 22.5 eV, producing positive ions that are measured using a quadrupole mass spectrometer. In these experiments, a mass spectrum with an m/z range of 10-500 was collected every second. In the experiments a small precisely controlled flow of argon (40 SCCM) mixed with helium carrier gas was used as a tracer gas to correct for drifts in the signal due to change in flow through the molecular beam inlet. This facilitated the qualitative comparison of relative concentrations among experimental conditions.

Laminar Entrained Flow Reactor (LEFR) Experiments. The laminar entrained flow reactor (LEFR) is a laboratory scale (10 g/h) biomass fast pyrolysis reactor (500 °C).<sup>32</sup> The reactor was constructed of 316 stainless steel tubing, 1.5 in. o.d. with a 0.065-in. wall, resulting in an i.d. of 1.37 in. The reactor length is 27 in. from the top of the heated zone to the inlet of the cyclone. The reactor is housed in a 4zone, resistively heated furnace rated to 1200 °C. A supervisory control and data acquisition (SCADA) system controls the process conditions to limit the wall temperature of the reactor to a maximum of 760 °C. For each zone, the furnace and wall temperature were controlled using proportional integral derivative (PID) controller algorithms in cascade mode. The LEFR midpoint and outlet gas

temperatures were controlled with a 1/16 in. K-type thermocouple and a third PID loop. Nitrogen was used as the carrier gas with primary flows into the biomass feeder and into the top of the reactor. Flows were adjusted to maintain a constant residence time independent of temperature, and a 0.1 psi pressure drop from the feeder to the reactor. The continuous biomass feed system (10 g/h) utilized a lockhopper system, allowing biomass to be reloaded and purged with nitrogen before feeding into the reactor. Biomass entering the reactor reacted and released volatile material and the residual char was collected. Char particles of sufficient size to avoid entrainment were collected in the bottom of the reactor, past the vapor outlet port, and were designated drop char. Fresh pyrolysis vapors and entrained char enter the outlet cyclone for separation to produce cyclone char. Only the drop char was utilized for this study.

Stereomicroscopy and Scanning Electron Microscopy (SEM). Whole biochar pieces retrieved from the LEFR were examined without further processing. A combination of reflected and transmitted light was used to generate high contrast images. Only the reflected light was used to determine char darkness values. Images were captured on a Nikon SMZ1500 stereomicroscope with a Nikon DS-Fil CCD camera operated by a Nikon Digital Sight system (Nikon Instruments, Melville, NY).

SEM imaging was performed using a FEI Quanta 400 FEG instrument under low vacuum (0.40-0.65 Torr) operating with the gaseous solid-state detector (GAD). Samples were mounted on aluminum stubs using carbon tape and sputter coated with 6 nm of gold. Imaging was performed at beam accelerating voltages from 12.5 to 25 keV.

Image Processing and Quantitative Analysis. ImageJ (National Institutes of Health, Bethesda, MD) was used to threshold images, segregate biomass and biochar particles from background and create a binary image. A custom MATLAB (MathWorks, Natick, MA, USA) script was used to generate the histograms and tables presented of the output from ImageJ. An illustration of the image processing and image analysis workflow is presented in Figure S1.

## ASSOCIATED CONTENT

#### Supporting Information

The Supporting Information is available free of charge on the ACS Publications website at DOI: 10.1021/acs.energyfuels.7b00791.

Figure S1, illustration of the image analysis workflow used to generate histograms of char particle darkness values from stereoscope reflected light images; Figure S2, histogram of darkness value distributions and corresponding statistics of 60-80 mesh pine char particles after pyrolysis at 550 °C (PDF)

# AUTHOR INFORMATION

#### **Corresponding Author**

\*Tel.: 303.384-7773. E-mail: bryon.donohoe@nrel.gov.

# ORCID

Peter N. Ciesielski: 0000-0003-3360-9210 Calvin Mukarakate: 0000-0002-3919-7977 Mark R. Nimlos: 0000-0001-7117-775X Bryon S. Donohoe: 0000-0002-2272-5059

The authors declare no competing financial interest.

# ACKNOWLEDGMENTS

This work was supported by the U.S. Department of Energy, Bioenergy Technologies Office (DOE-BETO) under contract number DE-AC36-08GO28308 with the National Renewable Energy Laboratory (NREL). The biochar image analysis work was supported as part of the Center for Direct Catalytic

Conversion of Biomass to Biofuels (C3Bio), an Energy Frontier Research Center funded by the U.S. Department of Energy, Office of Science, Office of Basic Energy Sciences, Award Number DE-SC0000997. Development of the particle-scale pyrolysis model was supported by the Consortium for Computational Physics and Chemistry (CCPC), funded by U.S. Department of Energy, Bioenergy Technologies Office (DOE-BETO).

# REFERENCES

- (1) Ragauskas, A. J.; Williams, C. K.; Davison, B. H.; Britovsek, G.; Cairney, J.; Eckert, C. A.; Frederick, W. J., Jr.; Hallett, J. P.; Leak, D. J.; Liotta, C. L.; Mielenz, J. R.; Murphy, R.; Templer, R.; Tschaplinski, T. The Path Forward for Biofuels and Biomaterials. *Science* **2006**, *311* (5760), 484–489.
- (2) Hoffert, M. I.; Caldeira, K.; Benford, G.; Criswell, D. R.; Green, C.; Herzog, H.; Jain, A. K.; Kheshgi, H. S.; Lackner, K. S.; Lewis, J. S.; Lightfoot, H. D.; Manheimer, W.; Mankins, J. C.; Mauel, M. E.; Perkins, L. J.; Schlesinger, M. E.; Volk, T.; Wigley, T. M. L. Advanced technology paths to global climate stability: Energy for a greenhouse planet. *Science* 2002, 298 (5595), 981–987.
- (3) Bridgwater, A. V.; Meier, D.; Radlein, D. An overview of fast pyrolysis of biomass. *Org. Geochem.* **1999**, *30*, 1479–1493.
- (4) Shafizadeh, F. Introduction to Pyrolysis of Biomass. J. Anal. Appl. Pyrolysis 1982, 3 (4), 283–305.
- (5) Czernik, S.; Bridgwater, A. V. Overview of applications of biomass fast pyrolysis oil. *Energy Fuels* **2004**, *18* (2), 590–598.
- (6) Morgan, T. J.; Kandiyoti, R. Pyrolysis of Coals and Biomass: Analysis of Thermal Breakdown and Its Products. *Chem. Rev.* **2014**, 114 (3), 1547–1607.
- (7) Shen, J.; Wang, X. S.; Garcia-Perez, M.; Mourant, D.; Rhodes, M. J.; Li, C. Z. Effects of particle size on the fast pyrolysis of oil mallee woody biomass. *Fuel* **2009**, *88* (10), 1810–1817.
- (8) Sage, R. F.; Peixoto, M. D.; Friesen, P.; Deen, B. C-4 bioenergy crops for cool climates, with special emphasis on perennial C-4 grasses. *J. Exp. Bot.* **2015**, *66* (14), 4195–4212.
- (9) Suliman, W.; Harsh, J. B.; Abu-Lail, N. I.; Fortuna, A. M.; Dallmeyer, I.; Garcia-Perez, M. Influence of feedstock source and pyrolysis temperature on biochar bulk and surface properties. *Biomass Bioenergy* **2016**, *84*, 37–48.
- (10) Babu, B. V.; Chaurasia, A. S. Heat transfer and kinetics in the pyrolysis of shrinking biomass particle. *Chem. Eng. Sci.* **2004**, *59* (10), 1999–2012.
- (11) Pang, J.; Zhang, J. Effects of gas temperature fluctuation on the instantaneous pyrolysis of biomass particles. *J. Anal. Appl. Pyrolysis* **2014**, *108*, 196–202.
- (12) Mettler, M. S.; Vlachos, D. G.; Dauenhauer, P. J. Top ten fundamental challenges of biomass pyrolysis for biofuels. *Energy Environ. Sci.* **2012**, 5 (7), 7797–7809.
- (13) White, J. E.; Catallo, W. J.; Legendre, B. L. Biomass pyrolysis kinetics: A comparative critical review with relevant agricultural residue case studies. *J. Anal. Appl. Pyrolysis* **2011**, *91* (1), 1–33.
- (14) Cetin, E.; Moghtaderi, B.; Gupta, R.; Wall, T. F. Influence of pyrolysis conditions on the structure and gasification reactivity of biomass chars. *Fuel* **2004**, *83* (16), 2139–2150.
- (15) Sadhukhan, A. K.; Gupta, P.; Saha, R. K. Modelling and experimental studies on pyrolysis of biomass particles. *J. Anal. Appl. Pyrolysis* **2008**, *81* (2), 183–192.
- (16) Sreekanth, M.; Kolar, A. K.; Leckner, B. Transient thermal behaviour of a cylindrical wood particle during devolatilization in a bubbling fluidized bed. *Fuel Process. Technol.* **2008**, 89 (9), 838–850.
- (17) Chen, L.; Dupont, C.; Salvador, S.; Grateau, M.; Boissonnet, G.; Schweich, D. Experimental study on fast pyrolysis of free-falling millimetric biomass particles between 800 degrees C and 1000 degrees C. Fuel 2013, 106, 61–66.
- (18) Pattanotai, T.; Watanabe, H.; Okazaki, K. Effects of particle aspect ratio on pyrolysis and gasification of anisotropic wood cylinder. *Fuel* **2015**, *150*, 162–168.

(19) Lu, H.; Ip, E.; Scott, J.; Foster, P.; Vickers, M.; Baxter, L. L. Effects of particle shape and size on devolatilization of biomass particle. *Fuel* **2010**, *89* (5), 1156–1168.

- (20) Wornat, M. J.; Hurt, R. H.; Davis, K. A.; Yang, N. Y. C. Single-particle combustion of two biomass chars. *Symp. (Int.) Combust.*, [Proc.] **1996**, 26 (2), 3075–3083.
- (21) Yu, J.; Lucas, J. A.; Wall, T. F. Formation of the structure of chars during devolatilization of pulverized coal and its thermoproperties: A review. *Prog. Energy Combust. Sci.* **2007**, 33 (2), 135–170.
- (22) Babu, B. V.; Chaurasia, A. S. Parametric study of thermal and thermodynamic properties on pyrolysis of biomass in thermally thick regime. *Energy Convers. Manage.* **2004**, *45* (1), 53–72.
- (23) Dufour, A.; Castro-Díaz, M.; Marchal, P.; Brosse, N.; Olcese, R.; Bouroukba, M.; Snape, C. In Situ Analysis of Biomass Pyrolysis by High Temperature Rheology in Relations with 1H NMR. *Energy Fuels* **2012**, *26* (10), 6432–6441.
- (24) Paulsen, A. D.; Hough, B. R.; Williams, C. L.; Teixeira, A. R.; Schwartz, D. T.; Pfaendtner, J.; Dauenhauer, P. J. Fast Pyrolysis of Wood for Biofuels: Spatiotemporally Resolved Diffuse Reflectance In situ Spectroscopy of Particles. *ChemSusChem* **2014**, 7 (3), 765–776.
- (25) Gable, P.; Brown, R. C. Effect of biomass heating time on bio-oil yields in a free fall fast pyrolysis reactor. *Fuel* **2016**, *166*, 361–366.
- (26) Ciesielski, P. N.; Crowley, M. F.; Nimlos, M. R.; Sanders, A. W.; Wiggins, G. M.; Robichaud, D.; Donohoe, B. S.; Foust, T. D. Biomass particle models with realistic morphology and resolved microstructure for simulations of intraparticle transport phenomena. *Energy Fuels* **2014**, 29 (1), 242–254.
- (27) Wiggins, G. M.; Ciesielski, P. N.; Daw, C. S. Low-order modeling of internal heat transfer in biomass particle pyrolysis. *Energy Fuels* **2016**, *30* (6), 4960–4969.
- (28) Di Blasi, C. Analysis of convection and secondary reaction effects within porous solid fuels undergoing pyrolysis. *Combust. Sci. Technol.* **1993**, 90 (5–6), 315–340.
- (29) Pecha, M. B.; Garcia-Perez, M.; Foust, T. D.; Ciesielski, P. N. Estimation of Heat Transfer Coefficients for Biomass Particles by Direct Numerical Simulation Using Microstructured Particle Models in the Laminar Regime. ACS Sustainable Chem. Eng. 2017, 5, 1046.
- (30) Ellens, C. J. Design, optimization and evaluation of a free-fall biomass fast pyrolysis reactor and its products. MSc. Thesis, Iowa State University, 2009.
- (31) Mukarakate, C.; Scheer, A. M.; Robichaud, D. J.; Jarvis, M. W.; David, D. E.; Ellison, G. B.; Nimlos, M. R.; Davis, M. F. Laser ablation with resonance-enhanced multiphoton ionization time-of-flight mass spectrometry for determining aromatic lignin volatilization products from biomass. *Rev. Sci. Instrum.* **2011**, *82*, 033104.
- (32) Jarvis, M. W.; Haas, T. J.; Donohoe, B. S.; Daily, J. W.; Gaston, K. R.; Frederick, W. J.; Nimlos, M. R. Elucidation of biomass pyrolysis products using a laminar entrained flow reactor and char particle imaging. *Energy Fuels* **2010**, 25 (1), 324–336.